# Erosion-corrosion behaviour of Zirconia, WC-6Co, WC-6Ni and SS316

**N. Andrews[a] , L. Giourntas[a] , A. M Galloway[a], A. Pearson[b]**

[a] Department of Mechanical & Aerospace Engineering, University of Strathclyde, Glasgow, Scotland

[b] Weir Engineering Services, Oil & Gas Division, East Kilbride, Glasgow, Scotland

## Abstract

The current study investigates a ceramic, two cermets and a metal under solid-liquid impingement with 3.5% NaCl and 150mg/l hydraulic fracturing sand at two extreme angles of impact, 90° and 20°. The materials tested were Zirconia, sintered WC-6Co, sintered WC-6Ni and SS316. Each material was exposed to a testing regime using re-circulating impinging jet apparatus with a velocity of 19m/s and one hour duration. The electrochemical properties of the materials were investigated in-situ through anodic and cathodic polarisation and application of cathodic protection. Post experimental analysis of the degraded surface was completed using Scanning Electron Microscopy (SEM) and Optical 3D Imaging. Zirconia exhibited a brittle response to erosion-corrosion testing with the mass loss at 90° being fifty times greater than the negligible mass loss at 20°. WC-6Co and WC-6Ni both outperformed SS316 under all solid-liquid impingement erosion-corrosion testing regimes. WC-6Ni exhibited slightly better erosion-corrosion resistance over WC-6Co at both 90° and 20°. SS316 had the best corrosion resistance and showed passivation during anodic polarisations in solid-liquid impingement conditions. The nickel binder increased the corrosion resistance of WC-6Ni over WC-6Co. Cathodic protection was successfully applied on sintered WC-6Co and SS316 isolating the key components of erosion-corrosion.

Keywords: *slurry erosion; cermets; steel; electrochemisty; surface analysis*

# 1. Introduction

Nowadays, engineering machinery with longer service lives are required to satisfy the current industrial demands. Erosion-corrosion is one of the most severe phenomenon that affects the performance of most hydraulic machinery. For this reason, research has been focused on the investigation of the wear performance of more complex and usually more expensive materials. The present erosion-corrosion behaviour study is concerned with high fracture toughness Zirconia ceramic, WC-6Co and WC-6Ni sintered tungsten carbide cermets, and SS316 austenitic stainless steel.

The materials under investigation each have attributes that suggest that they would present excellent erosion-corrosion resistance under solid-liquid impingement. Zirconia is a brittle ceramic with high hardness and high fracture toughness [1]. Ceramics offer the advantage of being immune to corrosion, isolating erosion as the single contributing factor towards material loss [2, 3]. Cermets such as sintered tungsten carbide claim the advantageous mechanical qualities of ceramics and metals. The high hardness and improved fracture toughness of sintered tungsten carbide-based cermets over ceramics have made them applicable to hard facing applications such as cutting tools, sand blasting nozzles, and a variety of other wear resistant applications [4]. SS316 is a ductile metal and is industrially recognised as a Corrosion Resistant Alloy (CRA). SS316 also offers the benefit of having a fracture toughness that is much higher than most other corrosion resistant metals and leads to an increased erosion-corrosion resistance as a result of it being able to absorb the impact momentum of the hydraulic fracturing sand and, thus, decreasing its susceptibility to brittle fracture.

The phenomenon of wear on a material's surface manifests itself in a number of forms such as friction, abrasion, erosion and erosion-corrosion. For hard-facing materials, such as ceramics and cermets, research has been primarily focused on friction, abrasion and erosion resistance [5-17] with extremely little published data on erosion-corrosion behaviour. Clark and Hawthorne [5] investigated the erosion resistance of a number of metallic coatings, cermets and ceramics including HVOF WC-12Co, HVOF WC-10Ni, SS316L and Alumina. The wear rate was determined in a Coriolis erosion tester which is designed to simulate low angle impact erosion in rapid test conditions. This research [5] concluded that materials

based on tungsten carbide had a greater erosion resistance than any other material under test. In particular the wear rate of WC-Co cermet was recorded as being approximately 1000 times lower than that of SS316L.

Ness and Zibbell [6] reviewed the abrasion and erosion resistance of WC-Co, Boron carbide and composite carbide under two different testing regimes. Dry erosion was investigated using silicon carbide abrasive at 90° angle of impingement. Abrasion resistance was tested using wet steel wheel abrasion with silica sand. Under these test conditions WC-Co showed two types of material removal, ductile ploughing and brittle fracture. On a microscopic level the degraded surface showed preferential removal of the softer cobalt binder material and thereafter the WC particles were unsupported and were uprooted. The preferential removal of the softer binder phase of cemented carbides has been confirmed by a number of different experimental techniques [4, 7-11, 17].

Hussainova [7] recorded the dry erosion resistance of WC-Co of binder composition 8-15% at impact angles 30°, 45°, 60°, 75° and 90° at velocities of 31, 61 and 80m/s indicating the response of this material to altering angle of impingement although the effect of corrosion was not considered. WC-Co exhibited the maximum erosion rate at $60^{o}$ which was stated as closer to the behaviour of ductile materials which have maximum erosion between 30 and 60 degrees [7]. Wentzel [4, 17] researched the development of tungsten carbide and the dependence of different binder compositions on erosion-corrosion performance at impingement angles of 45°, 60°, 75° and 90°. For the overall performance of the tested tungsten carbides the maximum erosion occurred at 75° angle of impingement. The Nickel binder presented greater passivation [17] corrosion resistance over the cobalt binder but had higher slurry erosion rates indicating that the mechanical properties of the material are more important than the corrosion resistance; erosion is the dominant factor in material loss.

Although, Zirconia is unaffected by corrosion, it is an important element of the total material loss of cermets and metals. Previous research into the electrochemical properties of tungsten carbide has been focused on its application as a type of coating to Stainless Steel and not in the sintered solid form which has not yet been reviewed [2, 18-19].

Building on previous research [20] this study assesses the overall erosion-corrosion performance of Zirconia, sintered WC-6Co, sintered WC-6Ni and SS316 using re-circulating impinging jet apparatus with fluid composed of 3.5% NaCl, to evoke corrosion, and 150mg/l hydraulic fracturing sand, to promote erosion. The erosion-corrosion resistance of each material at both 90° and 20° angle of impingement is discussed. The wear scar produced by the testing regime is analysed using Scanning Electron Microscopy (SEM) and Optical 3D Imaging and the findings will be discussed. The electrochemical properties of WC-6Co, WC-6Ni and SS316 are investigated through anodic polarisation, cathodic polarisation and cathodic protection. The effect of erosion, corrosion and interaction between erosion and corrosion were determined and therefore the relative importance of erosion and corrosion with regard to material loss at 90° angle of impingement will be discussed.

## 2. Experimental Methods

All Zirconia samples studied in this investigation were manufactured by powder metallurgy processing as were the sintered WC-6Co and WC-6Ni samples. All SS316 samples were prepared from cold rolled austenitic stainless steel bar stock. Pre-experimental analysis of the materials was undertaken using a Hitachi S-3700 Scanning Electron Microscope with a 20kV accelerating voltage and secondary electron detector.

The re-circulating impingement apparatus used to assess the erosion-corrosion resistance of the experimental materials is shown in the schematic, Figure 1. The rig comprises a pump which re-circulates fluid onto the surface of the specimen at constant velocity of 19m/s. The re-circulating fluid was composed of 3.5% NaCl and 150mg/l suspended hydraulic fracturing sand. The distribution of particle size is given in Table 1.

| Size (µm) | Percentage (%) |
|---|---|
| **≤250** | 2.5 |
| **251-420** | 18.4 |
| **421-500** | 50.7 |
| **501-600** | 23.3 |
| **≥601** | 5.1 |

**Table 1 : Distribution of particle size of solids used in liquid-solid slurry**

The angle of impingement was altered to obtain results for 90° and 20°. The nozzle diameter used was 3mm and was offset from the specimen by 5mm. The temperature increased from 13°C – 23°C during the one hour testing period. The conductivity and temperature were checked before and after the test. The exposed surface of each specimen was 11.34cm$^2$. Zirconia, WC-6Co and WC-6Ni were tested in the as-received condition with surface finishes which are illustrated in Table 2. SS316 was ground using incrementally finer grades of silicon carbide paper through 120, 220, 500 and 800grit. The specimens were washed in methanol immediately prior to a test. Each specimen was weighed prior and post-test using a mass balance with an accuracy of 0.1mg.

| Materials (as-received) | Surface Finish, Ra (µm) |
|---|---|
| **Zirconia** | 3.76 |
| **Sintered WC-6Co** | 3.37 |
| **Sintered WC-6Ni** | 3.45 |

**Table 2: As received roughness values**

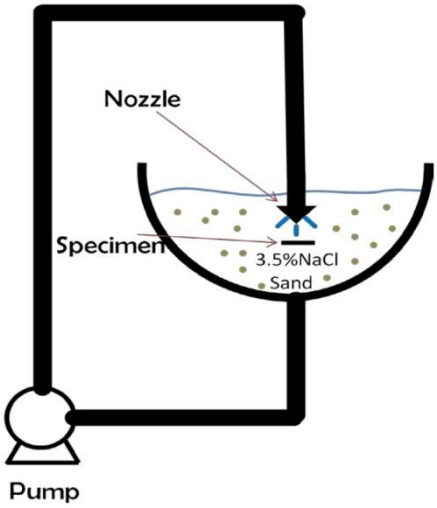


**Figure 1 : Schematic of erosion-corrosion rig**

In addition to mass loss experiments, electrochemical tests were conducted to understand the individual contribution of erosion, corrosion and the effect of corrosion on erosion, also known as synergy. The corrosion rate was measured in situ under solid-liquid impingement using a three-electrode electrochemical cell comprising a platinum counter electrode, Calomel electrode as the Reference Electrode and the material to be tested as the Working Electrode. Anodic Polarisation tests involved scanning the potential of the working

electrode from the free potential ($E_{corr}$) to the more positive potential at a sweep rate of 14mV/min. The tests were terminated when the electrode potential reached 50mV (SCE). Cathodic Polarisation tests involved a similar procedure to Anodic Polarisation except the potential was pressed from $E_{corr}$ to more negative potentials and the test was ceased when the electrode potential reached -1100mV (SCE).

Cathodic Protection was used to isolate erosion in potentiostatic conditions with the same test set-up as described above. Inspection of the polarisation plots indicated that the anodic reaction would be at an extremely low rate at electrode potentials more negative than -750mV (SCE). Hence the initial set of cathodic protection tests were undertaken at an impressed potential of -850mV. The instrument used for the electrochemical tests was ACM Instruments GillAC Serial No. 1734 using program Gill-AC Sequencer. Sequencer-Cyclic Sweep was used for anodic and cathodic polarisation and Sequencer-Potentiostatic for cathodic protection.

A post-test analysis was conducted to evaluate the exposed surface using an Olympus ZX51 light microscope and Hitachi S-3700 SEM. This enabled the micro-structural changes across the wear scar to be determined. The wear scar profile of each material was analysed using Infinite Focus Alicona Optical 3D imaging microscope.

# 3. Results

## 3.1. Material Characterisation

Typical mechanical and physical properties of each experimental material, provided by the supplier, are listed in Table 3. The particle size of both cermets was confirmed using SEM and found to be in the range of 1-3µm.

| Material | Composition | Density | Hardness | Fracture Toughness | Young's Modulus |
|---|---|---|---|---|---|
| **Zirconia** | 55.5% Zr, 25.5% C, 13.3% O, 4.7% N, 1.1% Mg | 5.6g/cm$^3$ | 1091HV | 7-8MPa.m$^{0.5}$ | 200GPa |
| **WC-6Co** | 93.85% WC, 0.1% VC, 6% Co | 14.95g/cm$^3$ | 1575HV | 10.7MPa.m$^{0.5}$ | 620GPa |
| **WC-6Ni** | 93.5% WC, 6% Ni, 0.5$Cr_3C_2$ | 14.85g/cm$^3$ | 1600HV | 12.1MPa.m$^{0.5}$ | 620GPa |
| **SS316** | Fe balance, 17% Cr, 12% Ni, 2.5% Mo, 1% Mn, 1.5% Si, 0.05% P, 0.04% S | 8.0g/cm$^3$ | 198HV | 195MPa.m$^{0.5}$ | 197.5GPa |

**Table 3 : Mechanical and Chemical Properties of all tested materials**

The chemical composition of each material was confirmed to be in accordance with the manufacturers values listed in Table 3. Microstructures of the sintered WC-6Co and WC-6Ni are shown in Figures 2 and 3. Both materials show rounded tungsten carbide particles with an even distribution of particle size. The binder content for both cermets is low at only 6%, therefore there is negligible definition of the binder material surrounding the tungsten carbide particles although elemental analysis confirms its presence. WC-6Co has a small quantity of larger, spherical tungsten carbide particles that are not present in WC-6Ni, Figure 2.

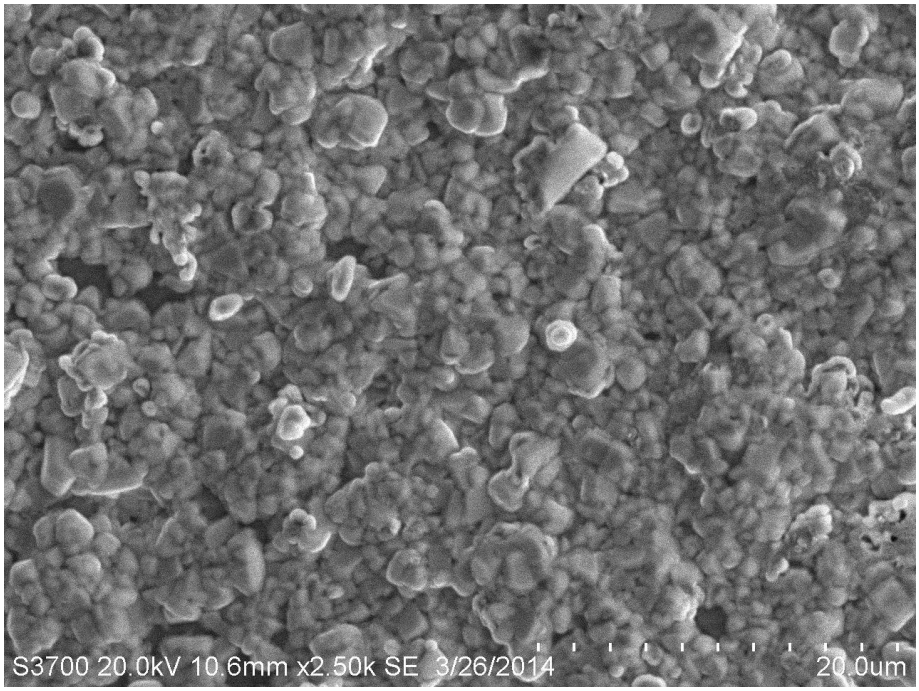


**Figure 2 : SEM images of WC-6Ni showing particle structure of WC particles**

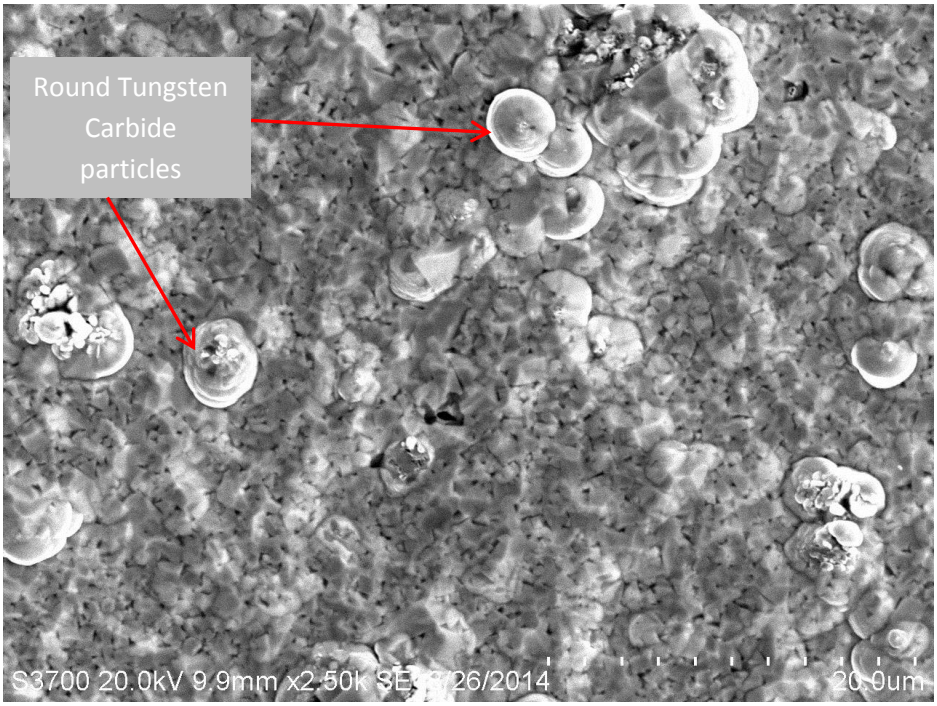


**Figure 3 : SEM image of WC-6Co showing particle structure of WC particles**

The microstructure of the powder metallurgy of Zirconia, with Magnesium Oxide stabiliser, was also determined using SEM after gold coating of the specimen. The microstructure is typical of a ceramic with an even distribution of pores due to the powder metallurgy process. The microstructure of Zirconia is shown in Figure 4.

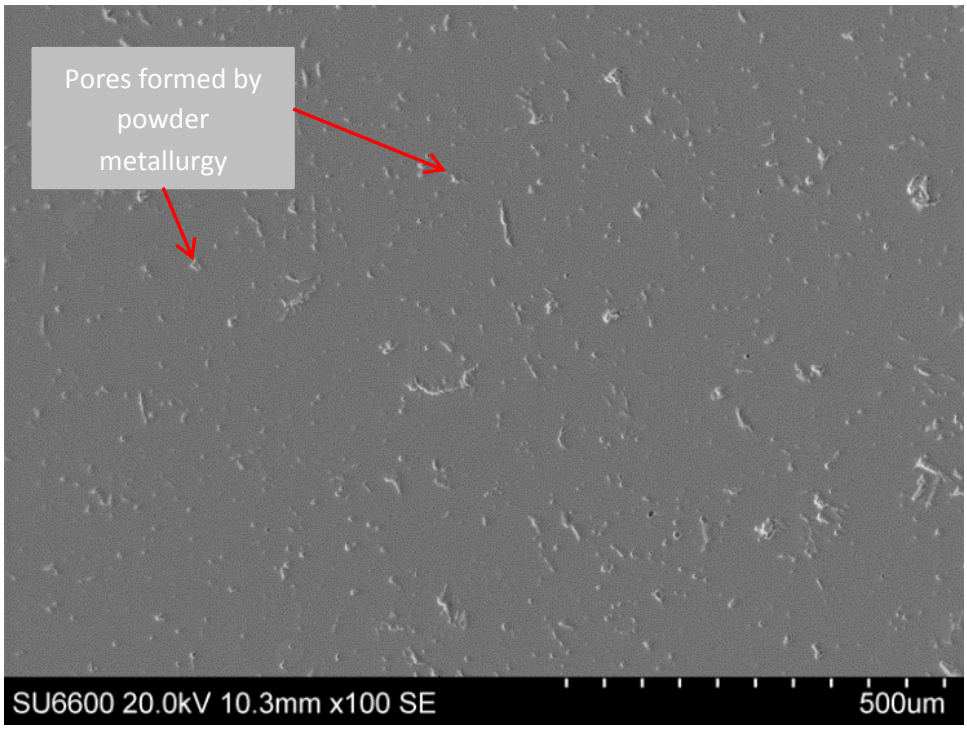


**Figure 4 : SEM image of Zirconia showing pore distribution from powder metallurgy process**

## 3.2. Erosion-corrosion material loss

### 3.2.1. Mass loss comparison

The effect of erosion-corrosion under flowing conditions was determined using the experimental procedure previously detailed. The results of each experiment are tabulated in Table 4; the averaged results are shown in Figure 5.

| Angle | Mass Loss/ mg | | | | | | | |
|---|---|---|---|---|---|---|---|---|
| | Zirconia | | WC-6Co | | WC-6Ni | | SS316 | |
| | Individual Replicates | Avg. | Individual Replicates | Avg. | Individual Replicates | Avg. | Individual Replicates | Avg. |
| **90°** | 18.1, 19.5, 20.5,18.4 | 19.1 | 1.8, 3.2, 2.3, 4.2 | 2.9 | 2.0, 2.1, 2.2, 2.3 | 2.2 | 3.8, 6.2, 3.5, 5.5, 5.4 | 4.9 |
| **20°** | 0.9, 0.4, 0.0 | 0.4 | 2.9, 2.3, 2.7, 3.0 | 2.7 | 0.3, 1.1, 0.7, 1.3 | 0.9 | 3.2, 4.5, 4.1, 5.1, 4.2 | 4.2 |

Table 4 : Compilation of test replicates with angle of impact

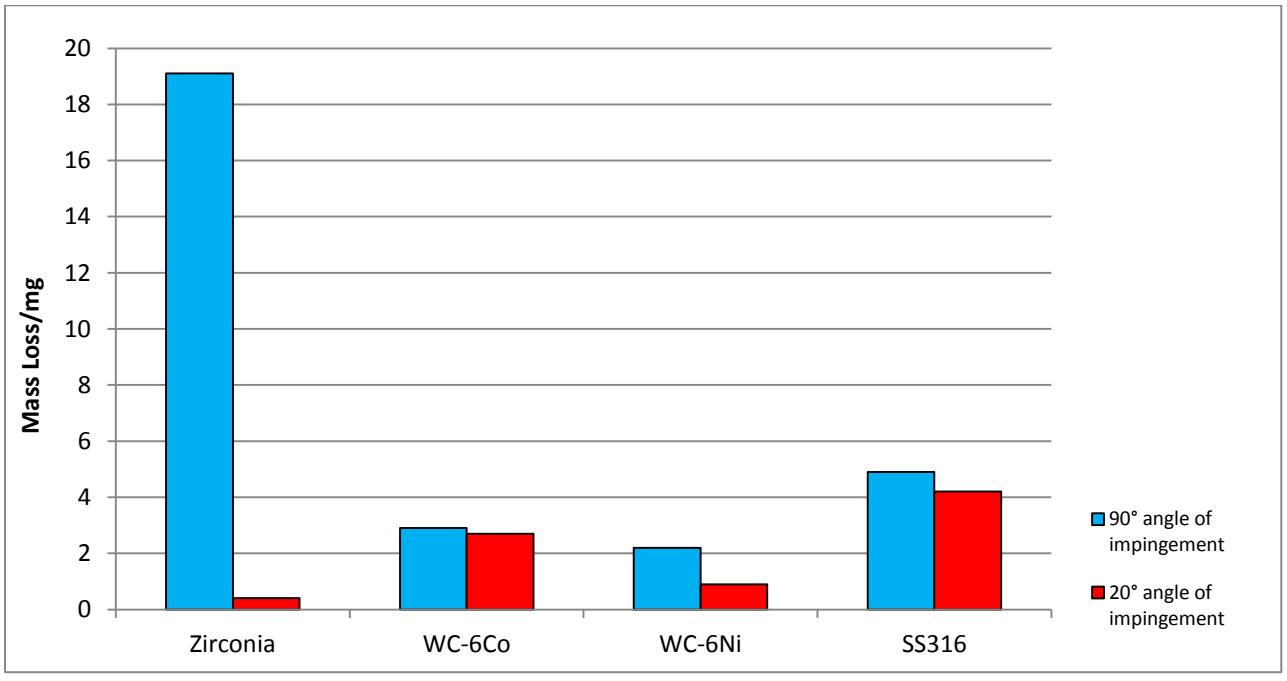


Figure 5 : Mass loss for each material at 20 degree and 90 degree angles of impingement

According to Figure 5, Zirconia is exhibiting a brittle response to altering angle of impingement. The mass loss at 90° angle of impact is approximately 50 times greater than

at 20° angle of impingement under the same erosion-corrosion conditions. Both cermets presented superior wear resistance at both angles of impingement in comparison to SS316. This is potentially because the hardness of WC-6Co and WC-6Ni are 1575 and 1600HV respectively in comparison with SS316 which is significantly less at 198HV. Referring to Figure 5, WC-6Ni has better wear resistance over WC-6Co at both angles of impact. Interestingly, WC-6Co presents similar mass loss at both 90° and 20° angle of impingement which is the trend shown by SS316. WC-6Ni has 2.5 times greater mass loss at 90° angle of impingement compared with 20° angle of impact. This indicates that WC-6Ni is presenting a more brittle response to altering angle of impingement but more experimental angles would need to be tested to confirm this.

## 3.3. Electrochemical Characteristics

### 3.3.1. Polarisation Plots

Anodic Polarisation and cathodic polarisation curves for WC-6Co, WC-6Ni and SS316 in flowing solid-liquid impingement conditions are shown in Figures 6 and 7. Zirconia is eliminated from this testing as it does not exhibit corrosion. The corrosion rate ($i_{corr}$) calculated by Tafel extrapolation are shown in Table 5. It can be deduced that the SS316 is the most corrosion resistant material tested followed by WC-6Ni and finally WC-6Co showing the least corrosion resistance.

| Material | Current ($i_{corr}$ )/ mA |
|---|---|
| **WC-6Co** | 0.25 |
| **WC-6Ni** | 0.16 |
| **SS316** | 0.06 |

**Table 5 : Corrosion rate of tested materials in solid-liquid impingement**

The curve showing the anodic polarisation of SS316 is of particular interest. The material is forming a passive oxide film which is being continually removed by the impinging solid particles. This is evident due to the oscillating current whilst the potential is pushed in the positive direction. After the electrode potential had reached -166mV the oscillations become less prominent and SS316 is actively corroding. WC-6Co and WC-6Ni do not appear to present any passivation in solid-liquid impingement conditions and are actively corroding throughout the entire test period.

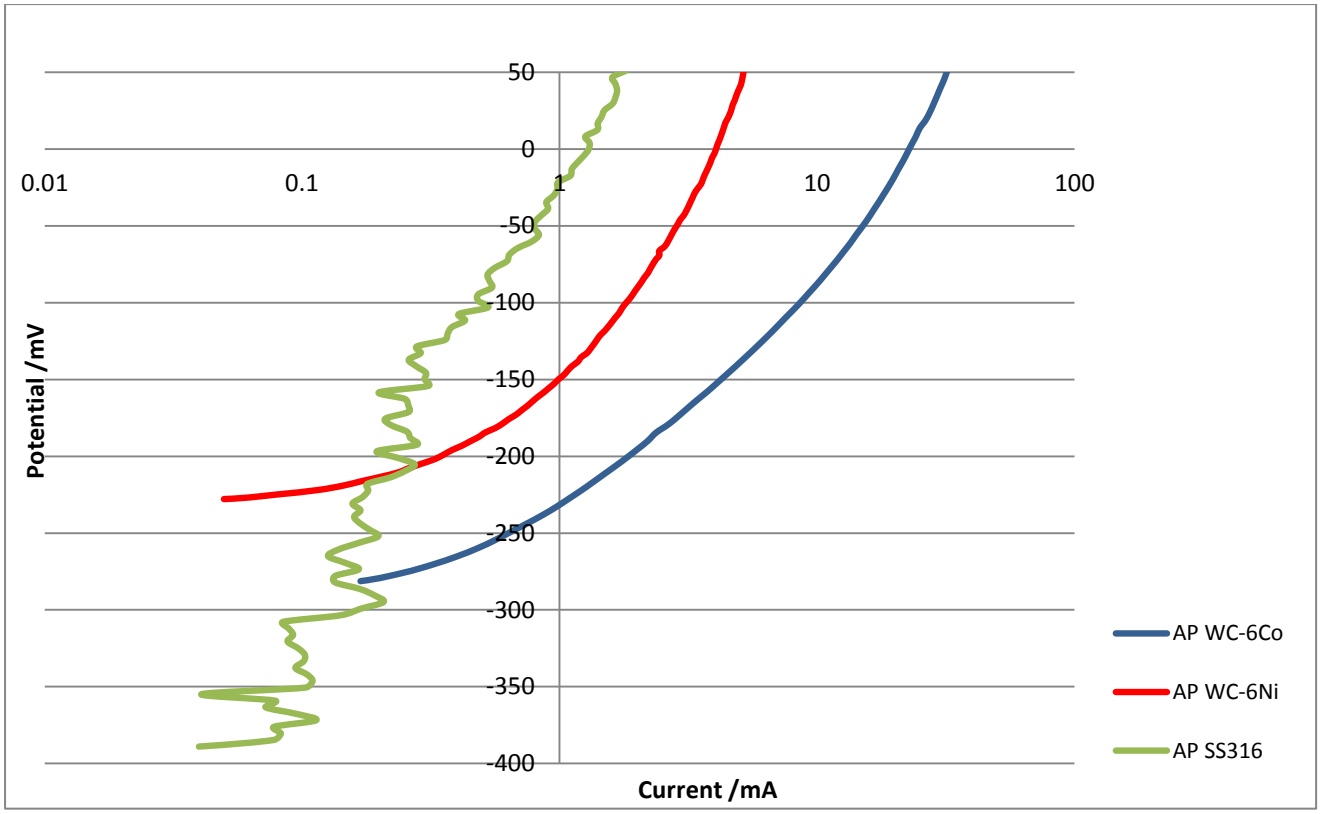


Figure 6 : Anodic Polarisation curves

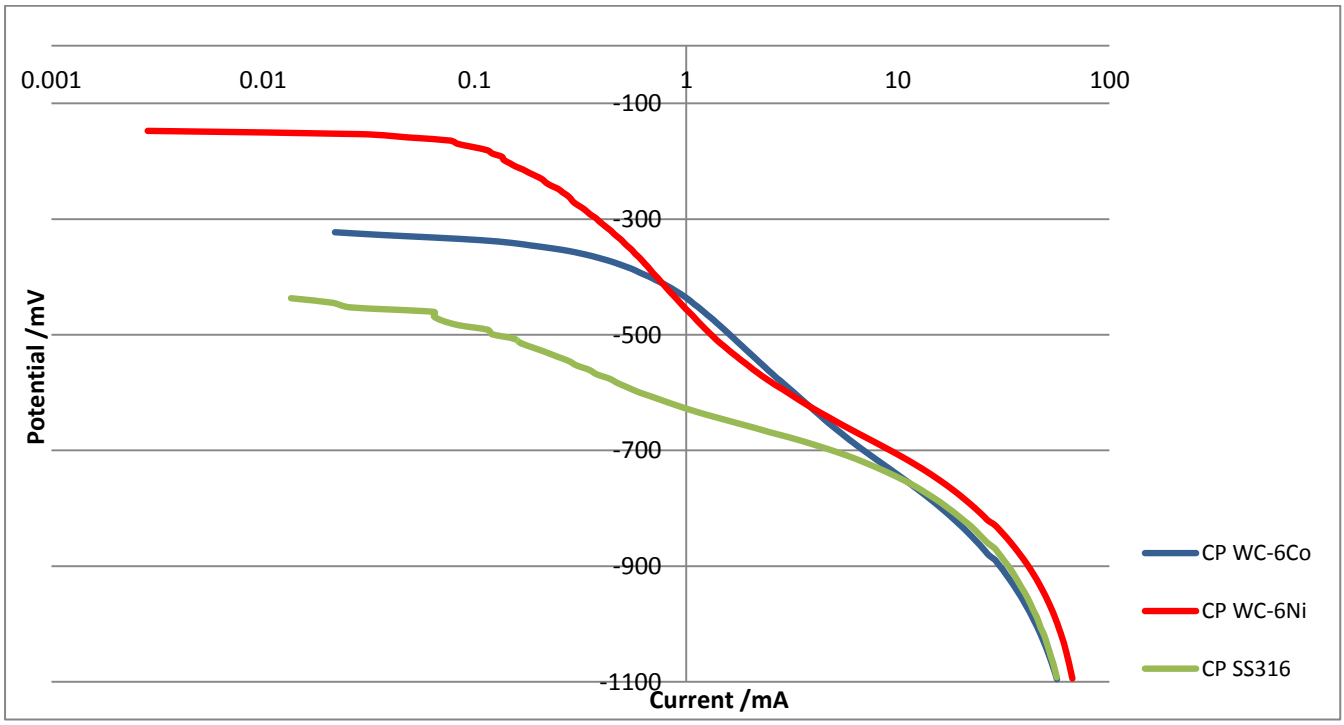


Figure 7 : Cathodic Polarisation Curves

### 3.3.2. Cathodic Protection

Figure 8, shows the effect of Cathodic Protection on WC-6Co, WC-6Ni and SS316. The potentiostatic tests were undertaken with a constant applied potential of -850mV (SCE). A decrease in mass loss is shown for WC-6Co and SS316 with the isolation of erosion. Based on Figure 8, the mechanism of erosion is a larger proportion of the total mass loss of WC-6Co in comparison with SS316.

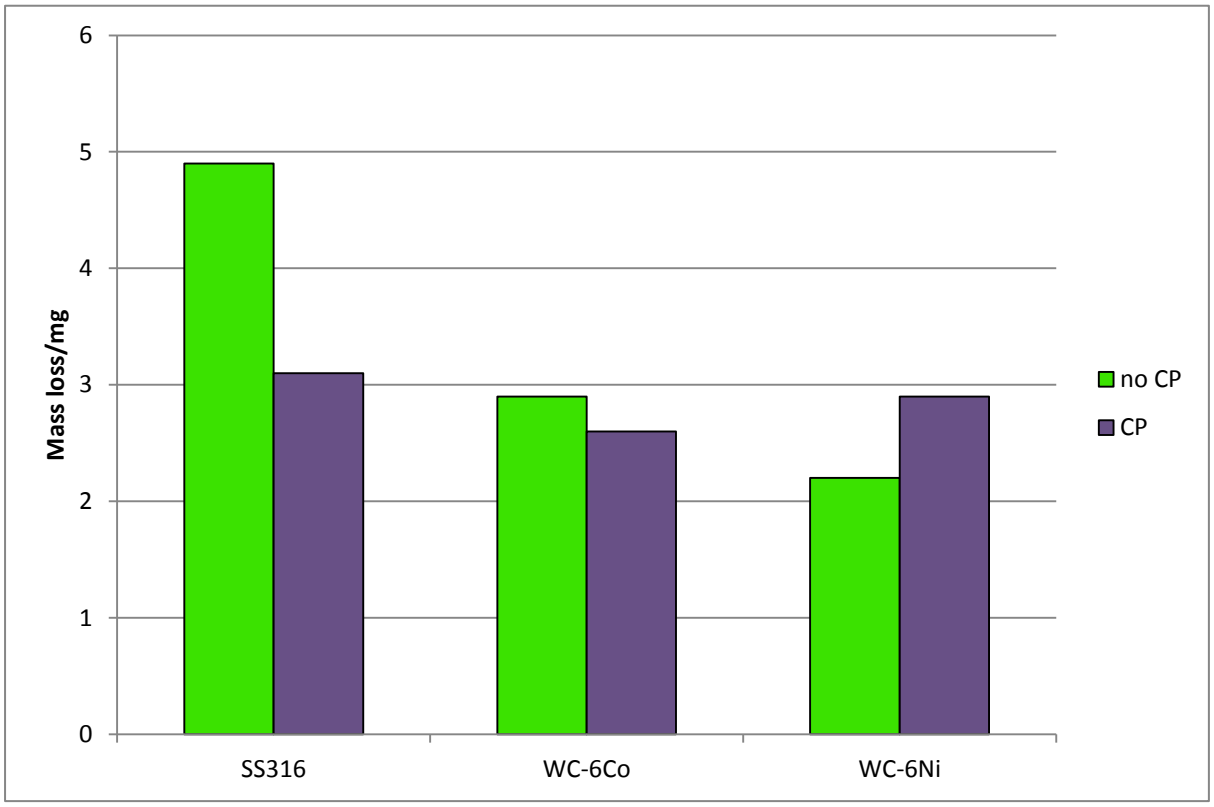


**Figure 8 : Cathodic Protection with applied potential -850mV**

Although, cathodic protection on sintered WC-6Co was effective WC-6Ni presents an increase in mass loss with the applied protection potential. The effect of corrosion should have effectively ceased beyond -800mV (SCE). Cathodic Protection is complex process and a by-product of applying a potential to the working electrode is that it may become susceptible to hydrogen embrittlement, a material degradation mechanism. Upon further investigation WC-6Ni is particularly sensitive to hydrogen embrittlement [21, 22]. Taking this into consideration, a number of different potentials were applied to the working electrode in order to determine if sintered WC-6Ni could effectively be protected by cathodic protection. Figure 9 shows that the mass loss was greater with all applied

potentials compared with the original erosion-corrosion testing with no cathodic protection. The complexities of these findings will be discussed in further detail later.

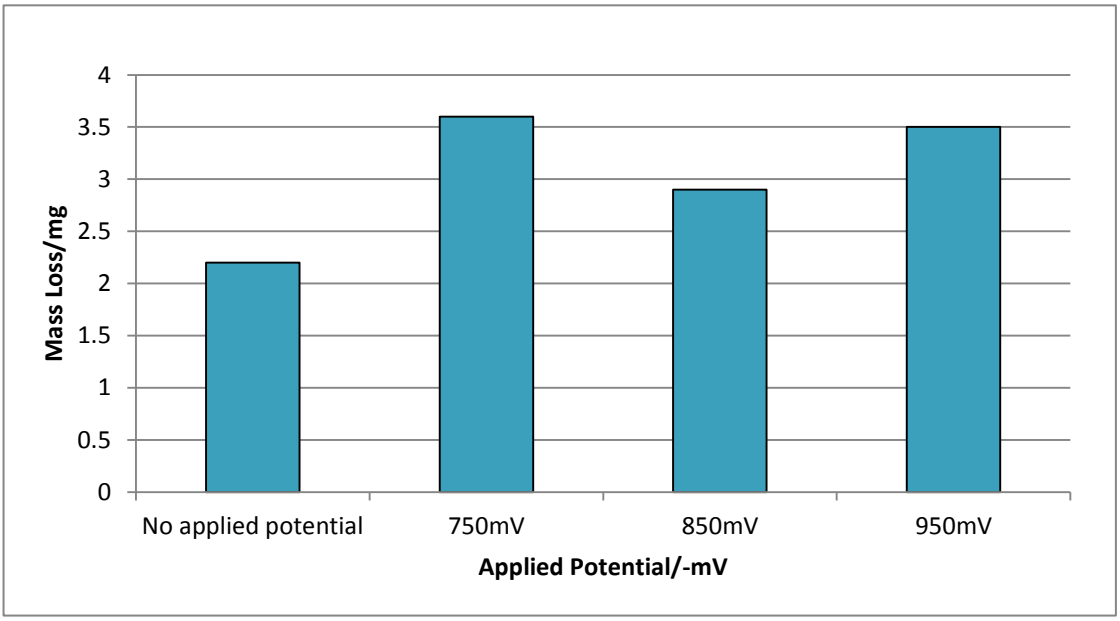


**Figure 9 : Varying applied potential of WC-6Ni**

## 3.4. Post-test analysis

### 3.4.1. Surface Topography

As the hydraulic fracturing sand particles are impacting on the surface the fracture toughness of the material will absorb the impacting momentum of the sand particles to prevent brittle fracture at the surface. The fracture toughness of Zirconia is the lowest compared with the other comparative materials. For this reason, Zirconia is most susceptible to brittle fracture under direct impingement. This is confirmed by the magnitude of mass loss recorded at 90° angle of impingement. Optical 3D Imaging was used to determine the wear scar profile; the profile of Zirconia, 90° angle of impact is shown in Figure 11.

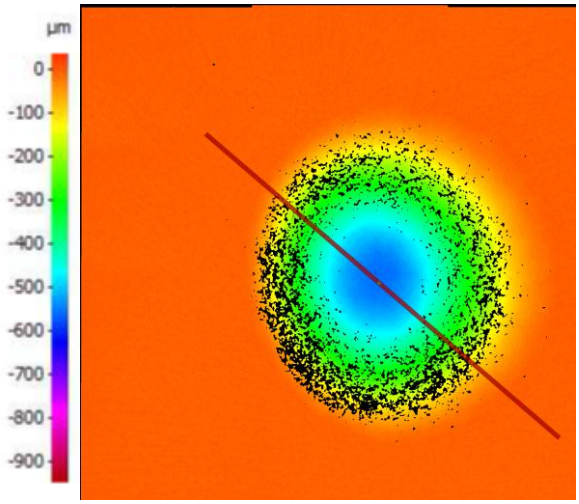


**Figure 10 : Surface Topography of Zirconia at 90° angle of impingement showing the distribution of wear scar depth across the surface**

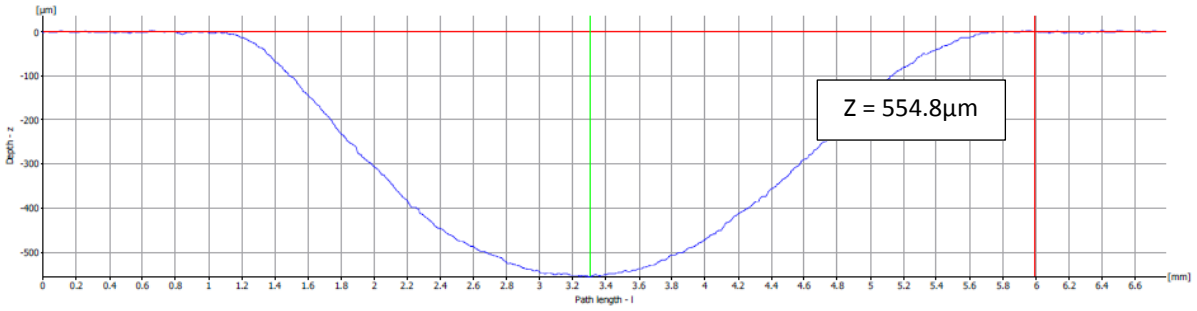


**Figure 11 : 2-D Wear scar profile of Zirconia at 90° angle of impingement showing the magnitude of wear scar depth**

The wear scar profile produced on SS316 at 90° angle of impact is shown in Figure 13. The magnitude of the wear scar depth is significantly decreased from Zirconia and the profile has increased roughness on the surface of the metal.

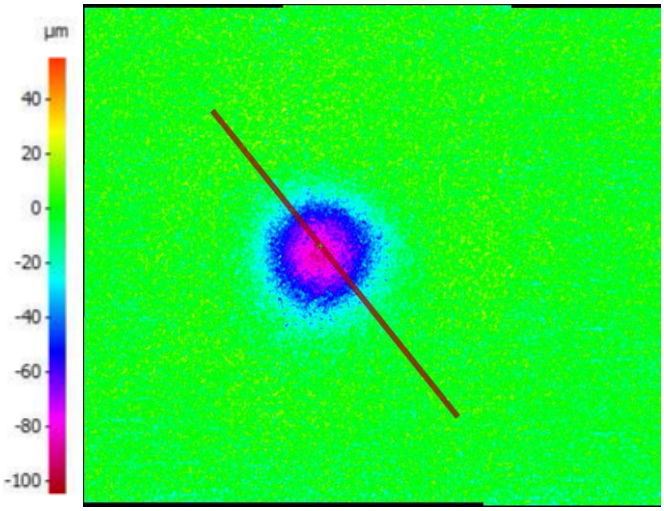


**Figure 12 : Surface Topography of SS316 at 90° angle of impingement showing the distribution of wear scar depth across the surface**

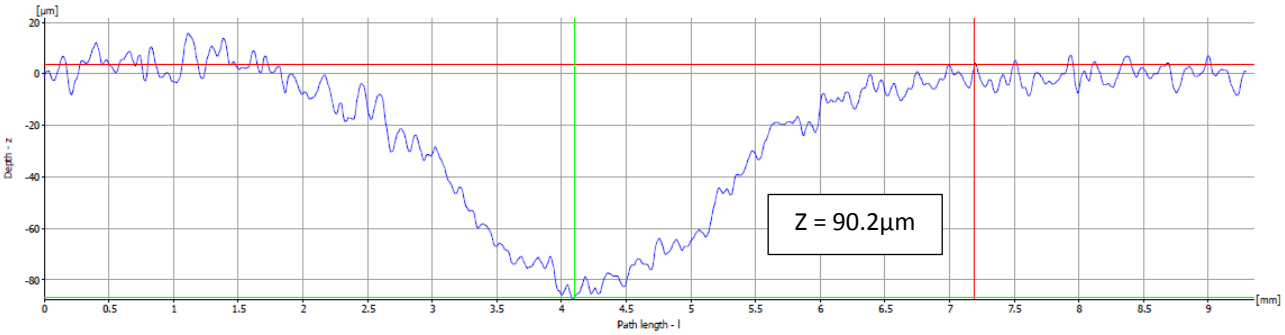


**Figure 13 : 2-D Wear scar profile of SS316 at 90° angle of impingement showing the magnitude of wear scar depth**

Table 6 correlates the wear scar depth over the degraded surface under erosion-corrosion impingement at 90° with the recorded mass loss. The two greatest recorded mass losses were profiled. At 20° angle of impingement on a macroscopic level the wear scar was not as evident as at 90° therefore useful data could not be compiled from Optical 3D Imaging.

| Material | Mass Loss/mg | Wear Scar Depth/µm |
|---|---|---|
| **Zirconia** | 19.5 | 510.4 |
| | 20.5 | 554.8 |
| **WC-6Co** | 3.2 | 23.3 |
| | 4.2 | 25.1 |
| **WC-6Ni** | 2.2 | 16.7 |
| | 2.3 | 24.5 |
| **SS316** | 5.4 | 103.9 |
| | 5.5 | 90.2 |

**Table 6 : Relationship of wear scar depths with mass losses at 90°**

As would be expected, there is a direct correlation between the mass loss and the wear scar depth. The wear scar depth of Zirconia is significantly greater than the other tested materials and proves that the usage of ceramics in wear resistant applications is potentially limited. Zirconia has a wear scar depth of approximately 5 times that of SS316 and up to 30 times that of the cermets. This result confirms that under direct impingement the usage of ceramics is inadvisable and cermets would be an advantageous choice with the same economic implications.

### 3.4.2. Wear Scar - Microstructural Analysis

Figures 14 and 15, show the microstructure of the degraded cermets post-experimental testing. The area analysed is located directly under the impingement jet where the greatest degradation of the surface will occur. The chemical composition was confirmed by taking a section analysis over the direct impingement area; the numerical results are shown in Table 6.

WC-6Ni appears to respond differently than WC-6Co in erosion-corrosion testing as the majority of the Nickel binder remains after testing, as shown in Table 7. This is potentially due to the superior corrosion resistance of Nickel in comparison to Cobalt as was confirmed by anodic polarisation. As the Nickel binder supports the tungsten carbide particles during erosion-corrosion testing the hard particles are less susceptible to particle pull-out which is

observable with WC-6Co, Figure 14. The hard tungsten carbide particles in both cermets appear more angular after erosion-corrosion testing. This is due to the bombarding hydraulic fracturing sand particles eroding the tungsten carbide particles prior to complete removal from the matrix. The same erosion-corrosion mechanism that is presented at 90°, Figures 14 and 15, remains true at 20°.

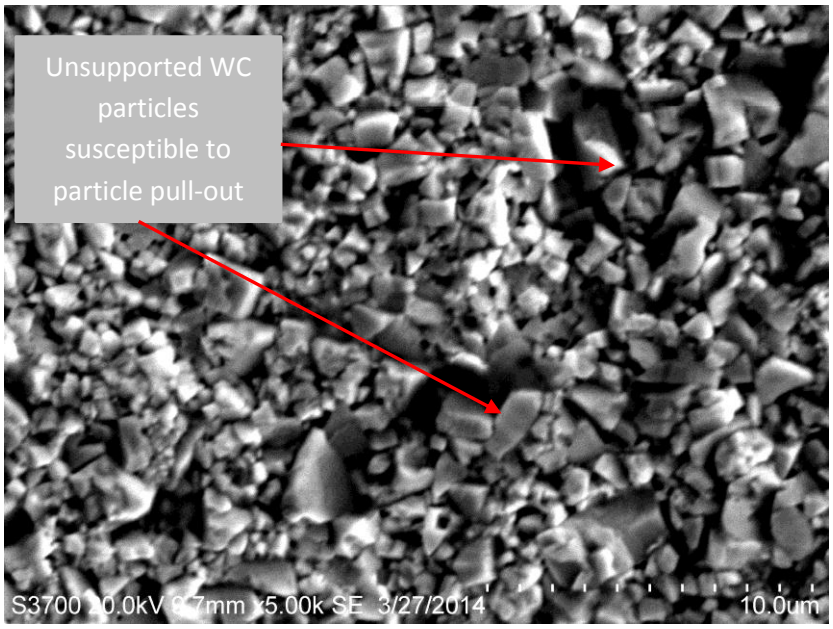


**Figure 14 : WC-6Co, 90° angle of impingement showing degraded micro-structure post erosion-corrosion testing**

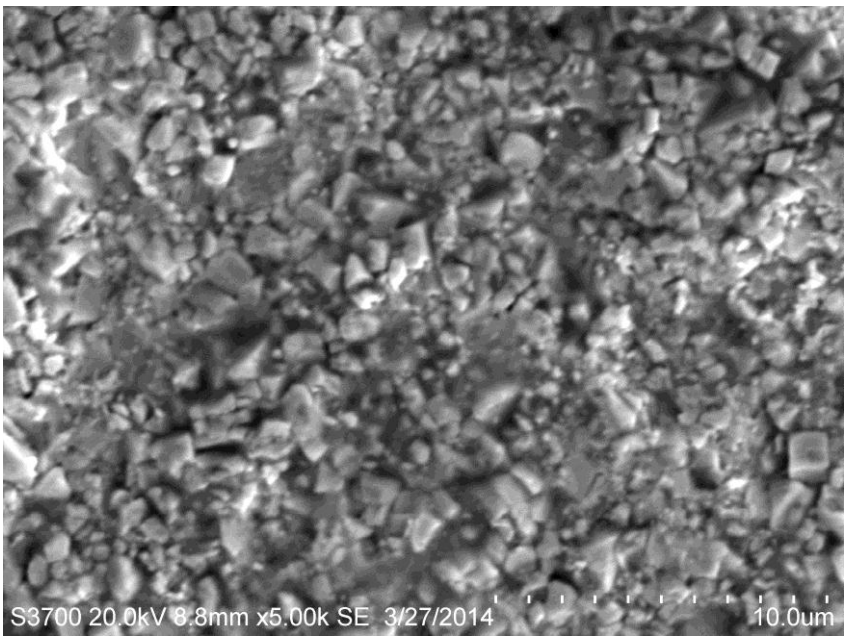


**Figure 15 : WC-6Ni, 90° angle of impingement showing degraded micro-structure post erosion-corrosion testing**

| Material | Angle/° | Binder Content/% |
|---|---|---|
| WC-6Co | 90 | 1.85 |
| | 20 | 2.31 |
| WC-6Ni | 90 | 5.31 |
| | 20 | 6.26 |

Table 7 : Binder content post-experimental testing

# 4. Discussion

This study has focused on the comparison of the erosion-corrosion resistance of a ceramic, two cermets and a metal. The areas in which each of the materials have excelled as well as been most susceptible to surface damage have been presented in the results section and they will be discussed further in this section.

## 4.1. Material loss experiments

The mechanical properties of a material are important in relation to erosion resistance. In this study, fracture toughness and hardness of materials were considered to explain the mass losses associated with the erosion-corrosion phenomenon. Zirconia, WC-6Ni, WC-6Co are all exceptionally hard with values greater than 1000HV but as a result have reduced fracture toughness. Comparatively, SS316 has significantly reduced hardness leading to higher fracture toughness, over 10 times greater than the other comparative materials. Under erosion-corrosion impingement if the material hardness exceeds that of impinging particles, the particles have difficulty removing material from the exposed surface [8]. High fracture toughness absorbs the impacting particles momentum decreasing the likelihood of brittle fracture at the materials surface. The superior erosion-corrosion resistance of the cermets over SS316 indicates that in this testing regime hardness is of greater mechanical importance than fracture toughness.

The ductile and brittle nature of the test materials was also considered as this is a major controlling factor in the response of a material to angle of impingement. Ceramics are classically brittle materials and as proved by the pioneering work of Finnie [23] exhibit the

greatest mass losses at 90°. Zirconia confirms this theory as the mass loss which was negligible at 20° is 50 times greater at 90° angle of impingement. At 20° the main mechanism of material loss is through sliding abrasion of the sand particles over the surface of the material, whereas at 90° the particles are directly impinging on the surface. The brittle nature of Zirconia is an important consideration with regard to its usage in hydraulic machinery; it could only be used in applications where sliding abrasion is the main deterioration mechanism.

WC-6Ni and WC-6Co are two-phase materials with a network of brittle tungsten carbides surrounded by a softer ductile metallic binder. The response to angle of impingement is therefore unknown although the small percentage composition of binder metal would indicate that the materials would degrade in a brittle manner. WC-6Co presents similar mass loss at both 90° and 20° angle of impingement in-line with the response of SS316. Austenitic Stainless Steels such as SS316 are considered ductile materials therefore by comparison could potentially indicate a greater ductile response of WC-6Co to angle of impingement. Alternatively, WC-6Ni has 2.5 times greater mass loss at 90° over 20°, indicative of a greater brittle response to angle of impingement. A greater variety of impingement angles would be required to verify the actual ductile or brittle response to angle of impact.

The brittle nature of Zirconia is also presented in the wear scar obtained through Optical 3D Imaging. It has been documented that in dry erosion at 90° angle of impingement brittle materials characteristically present U-shaped wear scars whereas ductile materials present W-shaped wear scars due to a stagnation point [23, 24]. Zirconia presents a smooth, deep (over 500µm) U-shaped wear scar indicative of a brittle response to erosion-corrosion testing. Difficulty was incurred when imaging the shallow (average 20µm) wear scars of WC-6Ni and WC-6Co due to the surface roughness of the two-phase materials. This has been previously established by D'Errico et al. who recorded that in erosion testing the crater morphology of ceramics was smooth whereas irregular fragmentation is observed in the case of cermets [12]. Austenitic Stainless Steels such as SS316 are characteristically ductile metals thus if the degradation laws relationship for dry erosion are upheld a W-shaped wear scar should have been presented. SS316 did not present a W-shaped wear scar in this testing regime. Previous research confirming the W-shaped wear scars used angular silica

sand as the erodent as opposed to round hydraulic fracturing sand used in this study [23, 24]. The interaction between the erodent and the material surface is dependent on the characteristics of the erodent and this is a potential reason for the lack of stagnation point presented with SS316.

The microstructure of the tested materials also played a pivotal role in determining the wear mechanisms occurring during the erosion-corrosion test. For each individual tested material the degradation of the microstructure at both 90° and 20° was similar which seems to be an interesting outcome. Zirconia, manufactured by powder metallurgy, showed severe degradation at 90° in the central impingement region where particulates are directly impacting on the surface. The area outside the direct impingement zone showed negligible degradation of the material. SS316 exhibited pitting and directionality in the outer impingement region but the central region for both angles the matrix was severely distorted. The main mechanism of material removal for WC-6Co is the preferential removal of the softer metallic binder phase. The hydraulic fracturing sand impacting on the surface removes the cobalt binder first by ductile ploughing which leaves the hard, brittle tungsten carbide particles exposed. This enables the solid particles to easily uproot the tungsten carbide particles from the microstructure. The material removal mechanism of WC-6Co has been previously documented and is characteristic of cermets [4, 7-11, 17]. Interestingly, preferential removal of the nickel binder does not occur with WC-6Ni during erosion-corrosion testing. Without the removal of the binder metal the tungsten carbide particles remain supported and thus are less susceptible to particle uprooting. This discovery can be attributed to the superior corrosion resistance of nickel over cobalt.

## 4.2. Electrochemical Characteristics

There are three contributing factors which combine to give the total mass loss for a material under erosion-corrosion testing: erosion, corrosion and synergy. In this study the electrochemical characteristics of WC-6Co, WC-6Ni and SS316 were investigated determining the individual contribution of each of these factors. Anodic Polarisations in solid-liquid impingement proved that SS316 has the greatest corrosion resistance followed by WC-6Ni and lastly WC-6Co. SS316 exhibited passivation and de-passivation of the metal oxide film under erosion-corrosion testing until the potential is pushed greater than -166mV

(SCE) and SS316 is actively corroding. WC-6Co and WC-6Ni do not exhibit any passivation and are actively corroding throughout the one hour testing period.

Application of Cathodic Protection at -850mV (SCE) was effective for SS316 and WC-6Co. This potential was effective to negate the corrosion component and isolate erosion. For both SS316 and WC-6Co the prevailing material degradation mechanism is erosion. The ratio of erosion to total mass loss for SS316 is E/TML = 0.63; for WC-6Co is E/TML = 0.90. WC-6Co has a greater proportion of the material loss due to erosion compared with SS316. With the application of CP at -850mV (SCE) the mass loss of WC-6Ni increased, with the ratio of erosion to total mass loss of E/TML = 1.32. The increased mass loss during the application of CP may be due to the susceptibility of the nickel binder to hydrogen embrittlement [21, 22]. Hydrogen embrittlement causes materials to reduce ductility and load bearing capacity by the ingress of hydrogen into the component. The reduced ductility of WC-6Ni increases brittle fracture at the surface of the material due to bombarding sand particles at 90° angle of impingement. The conventional standard applied potentials for CP in industrial applications are between -800mV (SCE) and lower to -1V (SCE). Further investigation was undertaken with WC-6Ni at potentials of -750mV (SCE) and -950mV (SCE) to determine if erosion could be isolated with sintered WC-6Ni around industrial standards. WC-6Ni continually showed an increase in mass loss with all applied potentials. This is an important discovery with regard to the applicability of sintered WC-6Ni in industrial applications where cathodic protection is going to be used as a wear prevention measure.

The individual contribution of Erosion (E), Corrosion (C) and Synergy (S) for SS316 and WC-6Co are shown in Table 8. The corrosion component was calculated using Tafel Extrapolation of the anodic polarisation curves, erosion component through cathodic protection, synergy is the remaining contribution. The electrochemical properties of the sintered tungsten carbides are controlled by the metallic binder phase and these Co/Ni corrosion characteristics were used in the determination of the corrosion component of the total mass loss.

| Material | E (%) | C (%) | S (%) |
|---|---|---|---|
| **WC-6Co** | 89.6 | 9.7 | 0.7 |
| **SS316** | 63.3 | 1.4 | 35.3 |

**Table 8 : Mass loss components**

The prominence of mechanical erosion in solid-liquid impingement is confirmed by the majority proportion of the total mass loss attributed to erosion as shown with both SS316 and WC-6Co. 'Synergy' played a key role in the erosion-corrosion performance of SS316. The elevated corrosion resistance reduces the proportion of the total mass loss which is contributed by corrosion. The two-phase cermet, WC-6Co, has 9.7% of the mass loss attributed to corrosion which is due to galvanic interactions between the tungsten carbide particles and the cobalt binder. Tungsten carbide particles act as the cathode and the cobalt binder acts as the anode in the electrochemical cell. As the composition of sintered cermets are 94% tungsten carbides and 6% Co/Ni binders the material is exhibiting large cathode/small anode theory which increases the corrosion rate above normal severity. Thus, the increase in the corrosion contribution enhances the susceptibility of mechanical damage due to erosion.

## 5. Conclusions

This study has demonstrated the following:

- Zirconia presents a classically brittle response to angle of impingement with the average mass loss at 90° being 50 times greater than mass loss at 20°.
- Cermets exhibited superior erosion-corrosion resistance over all comparative materials.
- The dominant mechanical feature which enhanced erosion-corrosion resistance in this testing regime was hardness of the material surface, confirmed by the superior performance of cermets over SS316.
- SS316 displayed greater pure corrosion resistance compared to the cermets indicating that mechanical properties are of greater importance than corrosion resistance in solid-liquid impingement.
- Sintered WC-6Ni exhibited the greatest overall wear resistance, with the nickel binder remaining in the microstructure after testing.
- CP application successfully protected SS316 and WC-6Co. On the other hand, sintered WC-6Ni could not be protected with conventional CP applied potentials due to Nickel binder's susceptibility to hydrogen embrittlement.
- Zirconia presented a deep, smooth U-shaped wear scar indicative of a brittle response at 90° angle of impingement.
- SS316 did not present an expected W-shaped wear scar at 90° angle of impingement. This due to the interaction of the hydraulic fracturing sand with the surface of the material.
- The contribution of erosion to the total mass loss is of greater proportion for WC-6Co compared to SS316.
- The 'synergistic' effect is of greater dominance with SS316 compared to WC-6Co.

## Acknowledgements

The authors would like to thank the Weir Group Limited for funding this project as well as Kyocera and Element 6 for provision of the ceramic and cermets respectively.

## References


1. Q. Fang, P. S Sidky, M. G. Hocking, Erosion and corrosion of PSZ-zirconia and the t-m phase transformation, Wear 233-235 (1999) 615-622.
2. T. Hodgkiess, A. Neville, S. Shrestha, Electrochemical and mechanical interactions during erosion-corrosion of a high-velocity-oxy fuel coating and a stainless steel, Wear 233-235 (1999) 623-634.
3. X. Hu, A. Neville, An examination of the electrochemical characteristics of two stainless steels (UNS S32654 and UNS S31603) under liquid-solid impingement, Wear 256 (2004) 537-544.
4. E. J Wentzel, The erosion-corrosion resistance of tungsten-carbide hard metals, International Journal of Refractory Metals and Hard Materials 15 (1997) 81-87.
5. H. McI Clark, H. M. Hawthorne, Y Xie, Wear rates and specific energies of ceramics, cermets and metallic coatings determined in the Coriolis erosion tester, Wear 233 (1999) 319-327.
6. E. Ness, R. Zibbell, Abrasion and erosion of hard materials related to wear in the abrasive waterjet, Wear 196 (1996) 120-125.
7. I. Hussainova, Some aspect of solid particle erosion of cermets, Tribology International 34 (2001) 89-93.
8. I. Hussainova, K. P. Schade, Correlation between solid particles erosion of cermets and particles impact dynamics, Tribology International 41 (2008) 323 – 330.
9. S. Okamoto, Y. Nakazono, K. Otsuka, Y. Shimoitani, J. Takada, Mechanical properties of WC/Co cemented carbide with larger WC grain size, Materials Characterization 55 (2005) 281-287.
10. J. Pirso, S. Letunovts, M. Viljus, Friction and wear behaviour of cemented carbides, Wear 257 (2004) 257-265.
11. D. H. Graham, A. Ball, Particle erosion of candidate materials for hydraulic valves, Wear 133 (1989) 125-132.
12. G. E. D'Errico, S. Bugliosi, D. Cuppini, Erosion of ceramics and cermets, Journal of Materials Processing Technology 118 (2001) 448-453.

13. Y. I. Oka, H. Ohnogi, T. Hosokawa, M. Matsumura, Impact-angle dependence and estimation of erosion damage to ceramic materials caused by solid particle impact, Wear 203-204 (1997) 573-579.
14. M. G. Gee, A. Gant, B. Roebuck, Wear mechanisms in abrasion and erosion of WC/Co and related hard metals, Wear 263 (2007) 137-148.
15. P. V. Krakhmalev, J. Sukumaran, A. Gaard, Effect of microstructure on edge wear mechanisms in WC-Co, International Journal of Refractory Metals and Hard Materials 25 (2007) 171-178.
16. I. Hussainova, J. Kubarsepp, J. Pirso, Mechanical properties and features of erosion of cermets, Wear 250 (2001) 818-825.
17. E. J. Wentzel, C. Allen, Erosion-corrosion resistance of tungsten carbide hard metals with different binder compositions, Wear 181-183 (1995) 63-69.
18. D. Toma, W. Brandl, G. Marginean, Wear and corrosion behaviour of thermally sprayed cermet coatings, Surface and Coatings Technology 138 (2001) 149-158.
19. V. A. Souza, A. Neville, Corrosion and erosion damage mechanisms during erosion-corrosion of WC-Co-Cr cermet coatings, Wear 255 (2003) 146-156.
20. N. Andrews, L. Giourntas, A. M. Galloway, A. Pearson, Effect of impact angle on the slurry erosion-corrosion of Stellite 6 and SS316., Wear (Under review)
21. R. J. H. Wanhill, S. A. Barter, S. P. Lynch, D. R. Gerrard, Prevention of hydrogen embrittlement in high strength steels, with emphasis on reconditioned aircraft components, RTO-AG-AVT 140 (2011) 20-1 - 20-52.
22. M. L. Martin, B. P. Somerday, R. O. Ritchie, P. Sofronis, I. M. Robertson, Hydrogen-induced intergranular failure in nickel revisited, Acta Materialia 60 (2012) 2739-2745.
23. I. Finnie, Erosion of surfaces by solid particles, Wear 3 (1960) 87-103.
24. D. Cooper, F. A. Davis, R. J. K Wood, Selection of wear-resistant materials for the petrochemical industry, J. Phys. D: Applied Physics 25 (1992) 195-204.